Ciliary neuropeptidergic signaling dynamically regulates excitatory synapses in postnatal neocortical pyramidal neurons

Lauren Tereshko[1], Ya Gao[1], Brian A. Cary[1], Gina G. Turrigiano[1,2], Piali Sengupta[1,2]

[1]Department of Biology

Brandeis University

Waltham, MA 02454

[2]Co-corresponding authors:

turrigiano@brandeis.edu

sengupta@brandeis.edu

ABSTRACT

Primary cilia are compartmentalized sensory organelles present on the majority of neurons in the mammalian brain throughout adulthood. Recent evidence suggests that cilia regulate multiple aspects of neuronal development, including the maintenance of neuronal connectivity. However, whether ciliary signals can dynamically modulate postnatal circuit excitability is unknown. Here we show that acute cell-autonomous knockdown of ciliary signaling rapidly strengthens glutamatergic inputs onto cultured neocortical pyramidal neurons, and increases spontaneous firing. This increased excitability occurs without changes to passive neuronal properties or intrinsic excitability. Further, the neuropeptide receptor somatostatin receptor 3 (SSTR3) is localized nearly exclusively to pyramidal neuron cilia both *in vivo* and in culture, and pharmacological manipulation of SSTR3 signaling bidirectionally modulates excitatory synaptic inputs onto these neurons. Our results indicate that ciliary neuropeptidergic signaling dynamically modulates excitatory synapses, and suggest that defects in this regulation may underlie a subset of behavioral and cognitive disorders associated with ciliopathies.

INTRODUCTION

Primary cilia are microtubule-based compartmentalized organelles that are present on nearly all mammalian cell types including neurons (Gerdes et al., 2009; Louvi and Grove, 2011). Cilia concentrate signaling molecules, and play critical roles in transducing environmental stimuli to regulate cellular properties (Bangs and Anderson, 2017; Elliott and Brugmann, 2019; Goetz and Anderson, 2010; Hilgendorf et al., 2016). Consequently, disruption of cilia and cilia-based signaling is causal to a set of pleiotropic disorders termed ciliopathies (Davis and Katsanis, 2012; Reiter and Leroux, 2017; Youn and Han, 2018). Abnormalities in brain development are a characteristic feature of many ciliopathies, highlighting the critical role of cilia in the nervous system (Guemez-Gamboa et al., 2014; Louvi and Grove, 2011; Valente et al., 2014; Youn and Han, 2018). Cilia have now been implicated in neurogenesis, neuronal migration, and establishment of synaptic connectivity during development (Baudoin et al., 2012; Chizhikov et al., 2007; Guo et al., 2017; Guo et al., 2019; Higginbotham et al., 2012; Higginbotham et al., 2013; Lee et al., 2020; Spassky et al., 2008; Willaredt et al., 2008). Intriguingly, cilia along with their complex signaling machinery are retained on mature neurons (Arellano et al., 2012; Guadiana et al., 2016; Sterpka and Chen, 2018), but whether ciliary signaling dynamically modulates mature neuronal properties has not been explored.

Recent studies have begun to implicate cilia in the establishment as well as maintenance of circuit connectivity and excitability in the postnatal brain. Loss of cilia and ciliary signaling results in defects in dendritic development and integration of adult born neurons into hippocampal circuits (Kumamoto et al., 2012). Disruption of ciliary signaling also reduces dendritic complexity and affects synaptic connectivity of interneurons in the postnatal striatum (Guo et al., 2017). Moreover, cilia loss in mature dentate granule cells leads to altered contextual

memory and synaptic plasticity at hippocampal mossy fiber synapses (Rhee et al., 2016). In a particularly interesting study, cilia in cerebellar Purkinje neurons were shown to be necessary for the maintenance of excitatory contacts from the climbing fibers of neurons in the inferior olivary nuclei of the medulla (Bowie and Goetz, 2020). In these reports, the effects on neuronal and circuit properties, and on synaptogenesis and synapse maintenance, manifested after prolonged (weeks to months) loss of cilia and/or ciliary signaling in the postnatal brain. Whether ciliary signaling can modulate synaptic properties on a more rapid timescale to adjust neuron and circuit excitability is unknown.

Neuronal cilia in different brain regions specifically localize a diverse set of neuropeptide and neurotransmitter receptors. Cilia-localized receptors in the brain include serotonin receptor 6, melanin-concentrating hormone receptor 1, somatostatin receptor 3 (SSTR3), and dopamine receptors D1, D2 and D5 among others (Berbari et al., 2008a; Brailov et al., 2000; Domire et al., 2011; Hamon et al., 1999; Handel et al., 1999; Loktev and Jackson, 2013; Marley and von Zastrow, 2010; Schulz et al., 2000). Signaling via these ciliary receptors is proposed to be mediated in part via regulation of adenylyl cyclase 3 (AC3) and the cAMP second messenger. Similar to the localization patterns of these receptors, AC3 is also specifically enriched in the cilia of diverse neuron types in the brain (Berbari et al., 2007, Guadiana 2016; Bishop et al., 2007). Mutations in these receptors and AC3 are associated with a range of cognitive, metabolic, and behavioral disorders that are hallmarks of many ciliopathies (Chen et al., 2016; Einstein et al., 2010; Lee and Gleeson, 2011; Loktev and Jackson, 2013; Wang et al., 2011; Youn and Han, 2018). These receptors continue to be expressed in neuronal cilia in adults, and many of the cognate neurotransmitter and neuropeptide ligands are released locally by neurons or modulatory

inputs, suggesting that cell-cell signaling through cilia-localized receptors plays an important role in the postnatal brain.

Neuronal circuits must maintain excitability within narrow bounds to prevent signal saturation or silencing (Turrigiano and Nelson, 2000), but the mechanisms that establish and dynamically maintain circuit excitability over a wide range of temporal and spatial scales are incompletely understood (Turrigiano, 2017). Several ciliopathies manifest with symptoms consistent with imbalances in excitability, such as cognitive impairment and recurrent epileptic seizures (Guemez-Gamboa et al., 2014; Lee and Gleeson, 2011; Novarino et al., 2011). These observations suggest the intriguing hypothesis that ciliary signaling plays an important role in adjusting neuronal excitability, either by altering intrinsic excitability through modulation of ion channel function or distribution, or by regulating the properties of excitatory or inhibitory synapses. The notion that neuropeptide and neurotransmitter release might converge on cilia to dynamically adjust intrinsic or synaptic properties, and thus modulate circuit excitability, has not been explored.

Here, we show that disruption of cilia and ciliary signaling in individual postnatal cortical pyramidal neurons in primary neuronal culture rapidly (<24 hrs) and cell-autonomously strengthens excitatory synapses onto these neurons. Consistent with enhanced excitatory transmission, acute loss of cilia results in increased neuronal firing without affecting intrinsic neuronal excitability. In contrast to previous findings from chronic cilia disruption, acute cilia disruption has no major impact on dendritic arborization. We find that the SSTR3 neuropeptide receptor is specifically localized to the cilia of cortical pyramidal neurons but not inhibitory interneuron subtypes, and that an SSTR3-selective antagonist and agonist bidirectionally modulate excitatory synaptic properties over similarly rapid timescales. Our results indicate that

neuropeptidergic signaling via cilia-localized receptors dynamically modulates synaptic strength, and plays a critical role in regulating neuronal excitability in the postnatal mammalian brain.

RESULTS

Neuronal morphology is unaffected upon acute disruption of ciliary signaling in the postnatal cortex

Ciliogenesis in neocortical pyramidal neurons occurs progressively during early postnatal development, beginning at birth, with cilia reaching maximal lengths after several weeks (Arellano et al., 2012). To assess the development of cilia in cultured postnatal cortical neurons, we dissociated neurons from visual cortex of Long-Evans rat pups at postnatal days 0-1 (P0-1), and plated them onto beds of confluent astrocytes as described previously (Pratt et al., 2003; Tatavarty et al., 2020). After eleven days *in vitro* (DIV), the majority of cortical neurons extended a single primary cilium from their soma, as assessed via staining with the neuronal cilia markers ARL13B and AC3 (Figure 1A,B) (Berbari et al., 2007; Bishop et al., 2007; Caspary et al., 2007; Sipos et al., 2018). To ask whether cilia distribution and length are similar between excitatory and inhibitory neurons, we quantified the percentage of GAD67-positive (inhibitory interneurons) and GAD67-negative (excitatory) neurons containing cilia. Approximately 90% of both cell types exhibited cilia of lengths similar to those of postnatal neocortical neurons *in vivo* (Arellano et al., 2012) (Figure 1A-C). Cilia lengths varied as expected (Arellano et al., 2012), but were similar across cell types (Figure 1C). These observations indicate that both excitatory and inhibitory postnatal cortical neurons contain primary cilia in culture at DIV11.

Since dendritic arbors are dynamic in these young postsynaptic neurons (Pratt et al., 2008; Pratt et al., 2003), we asked whether acute perturbation of ciliary signaling impacts

dendritic morphology. To perturb cilia in a cell-autonomous manner, we transfected DIV9-10 cortical cultures at low efficiency (5-10 neurons transfected/dish) with GFP alone, or GFP and one of two shRNAs targeting the ciliary small GTPase Arl13b (shArl13b_1 and shArl13b_2). In this and all further experiments, GFP was used to identify and target transfected neurons for immunohistochemical or electrophysiological analysis. Mutations in Arl13b have been shown to affect ciliary signaling without fully truncating cilia (Caspary et al., 2007; Cevik et al., 2010; Larkins et al., 2011; Lu et al., 2015). Pyramidal neurons transfected with either shRNA for 24 hrs showed a reduction in total immunolabeled ARL13B fluorescence in cilia by ~50% as compared to non-transfected control cells (Figure 1D,E), indicating that both shRNAs were effective at rapidly knocking down ARL13B (henceforth referred to as acute knockdown). This reduction in ARL13B was sufficient to shorten cilia (assessed using AC3 fluorescence) in these postnatal pyramidal neurons (Figure 1F), as reported previously in other cell types (Caspary et al., 2007; Cevik et al., 2010; Larkins et al., 2011; Lu et al., 2015). However, in contrast to the significant reduction in dendritic complexity observed upon prolonged conditional Arl13b deletion in striatal interneurons (Guo et al., 2017), acute and cell-autonomous knockdown of ARL13B for 24 hrs or 48 hrs had no impact on the total length of apical-like dendrites, or on the number of dendritic branch points (Figure 1G-I, Figure 1 – figure supplement 1A-C).

Since knockdown of ARL13B affects ciliary signaling but does not fully truncate cilia (Caspary et al., 2007; Higginbotham et al., 2012; Higginbotham et al., 2013), we tested whether more severe disruption of cilia structure is sufficient to rapidly alter neuronal morphology. The basal body component CEP164 and the intraflagellar transport protein IFT88 are essential for ciliogenesis and cilia maintenance (Graser et al., 2007; Pazour et al., 2000). Co-expression of shRNAs targeting both genes reduced IFT88 fluorescence by ~70% as assessed by

immunostaining (Figure 1- figure supplement 1D,E), and resulted in severely truncated cilia within 48h of transfection (Figure 1- figure supplement 1F). However, despite the dramatic disruption of cilia structure, we again observed no gross effects on pyramidal neuron morphology (Figure 1- figure supplement 1A-C). We conclude that acute cilia disruption does not strongly impact postnatal pyramidal neuron dendritic morphology.

Acute knockdown of ARL13B selectively strengthens excitatory synapses

Conditional, prolonged depletion of ARL13B at postnatal stages alters not only morphology but also connectivity of striatal interneurons (Guo et al., 2017). Moreover, cilia disruption for weeks to months induces loss of climbing fibers synapses onto Purkinje cells, and reduces synaptic integration of adult-born dentate granule cells (Bowie and Goetz, 2020; Kumamoto et al., 2012). We wondered whether acute and cell-autonomous disruption of cilia function is sufficient to regulate the strength or number of excitatory and/or inhibitory synapses on a more rapid timescale.

To address this issue, we acutely disrupted cilia via transfection of shArl13b, or cotransfection of shCep164 and shIft88, into DIV9-10 cultured pyramidal neurons. We then fixed and immunostained these cultures using antibodies against the excitatory presynaptic marker VGlut1, and the postsynaptic AMPA-type glutamate receptor subunit GluA2 (AMPA receptor: AMPAR) under non-permeant conditions to label surface receptors; sites of colocalization are considered putative excitatory synaptic sites (Figure 2A,B). Manipulation of cilia signaling using either method increased the intensity of surface synaptic GluA2; this increase was evident at both 24 hrs and 48 hrs after transfection (Figure 2C), indicating that reducing ciliary function increases the synaptic accumulation of AMPAR. Postsynaptic reduction

of cilia function with shArl13b_1 also increased presynaptic expression of VGlut1, although this change was less robust (Figure 2- figure supplement 1A). Quantification of the density of putative excitatory synapses along dendritic arbors also revealed a significant increase in excitatory synapse density that was evident at 48 hrs after knockdown (Figure 2D). Thus, acute and cell-autonomous cilia disruption increases both the number of excitatory synapses and the accumulation of synaptic AMPAR. Together, these changes are predicted to enhance excitatory synaptic drive.

Since the balance between excitation and inhibition (E/I balance) is determined by the relative drive from glutamatergic and GABAergic neurons, we next asked whether ciliary signaling also impacts inhibitory synapses. Different inhibitory interneuron subtypes preferentially synapse onto different compartments of cortical pyramidal neurons (Kepecs and Fishell, 2014; Tremblay et al., 2016; Urban-Ciecko and Barth, 2016). Somatic synapses are difficult to quantify in culture due to the density of somata, so we focused on the more readily quantifiable inhibitory synapses that contact the apical-like dendrites of pyramidal neurons. We used colocalization of GAD65 (a presynaptic inhibitory marker) and Gephyrin (a postsynaptic inhibitory marker) to identify putative inhibitory synapses (Figure 2E); we observed no significant change in the fluorescence intensities of either marker after cilia disruption (Figure 2E,F, Figure 2 – figure supplement 1B). Inhibitory synapse density was also unaltered following acute cilia disruption (Figure 2G). We infer that ciliary signaling acutely regulates excitatory, but not inhibitory, synapses onto cultured postnatal pyramidal neurons.

Increased accumulation of surface AMPAR at synaptic sites is predicted to increase the postsynaptic strength of excitatory synapses. To test this, we used whole cell voltage clamp in the presence of tetrodotoxin, APV, and picrotoxin to record AMPA-mediated miniature

excitatory postsynaptic currents (mEPSCs) from DIV11 control or shArl13b-transfected neurons (Figure 3A, left). Consistent with strengthened excitatory synapses, neurons whose cilia were acutely disrupted had larger mean mEPSC amplitudes compared to transfected controls (Figure 3A, right). Analysis of the cumulative probability distribution function of individual events showed that both manipulations shifted the amplitude distributions toward larger values (Figure 3B). mEPSC frequency is quite variable in culture, and was not significantly affected by cilia disruption at 24 hrs (Figure 3C). Neither resting membrane potential nor input resistance was altered (Figure 3D,E), indicating that acute knockdown of ARL13B has no effect on passive electrical properties. These results indicate that ciliary signaling acts cell-autonomously to rapidly increase excitatory postsynaptic strength.

Acute knockdown of ARL13B increases spontaneous firing without affecting intrinsic excitability

Increasing excitatory synapse number and strength without a concomitant change in inhibitory synapses would be expected to increase net excitatory synaptic drive. We thus investigated whether knockdown of ARL13B increases spontaneous firing. To test this, we performed whole cell patch clamp recordings in current clamp under conditions where synaptic inputs are intact and drive spontaneous firing (Figure 4A). To compensate for differences in resting potential across neurons, a small DC current was injected to maintain the inter-spike membrane potential close to -55 mV (see Methods). We targeted control or knockdown GFP-transfected neurons, recorded spontaneous firing, and calculated the firing rate. As expected, we observed a broad distribution of mean firing rates (Trojanowski et al., 2020; Turrigiano et al.,

1998); this distribution was shifted toward larger values after acute ARL13B knockdown, such that mean firing rate roughly doubled upon this manipulation (Figure 4A, right).

In addition to enhanced excitatory synaptic drive, increased intrinsic excitability could also potentially contribute to enhanced spontaneous firing. To determine whether cilia disruption impacts the intrinsic excitability of pyramidal neurons, we recorded under conditions where excitatory and inhibitory synaptic inputs were pharmacologically blocked (see Methods), and then injected direct current steps from -65 mV to evoke spikes and examine current vs firing rate (FI) curves. Knockdown of ARL13B had no significant impact on the FI curve (Figure 4B). Taken together with the lack of an effect on passive neuronal properties and dendritic arborization, these data show that intrinsic neuronal excitability and morphology are unaffected by acute and cell-autonomous manipulation of cilia. Instead, the increase in spontaneous firing is likely driven by the increase in number and strength of excitatory synapses.

The SSTR3 neuropeptide receptor is largely restricted to the cilia of excitatory neurons in the postnatal cortex

Cilia specifically localize multiple neuropeptide receptors, a subset of which has been implicated in the regulation of neuronal and circuit properties in the developing and mature brain (Einstein et al., 2010; Guo et al., 2017; Hilgendorf et al., 2016; Loktev and Jackson, 2013; Mykytyn and Askwith, 2017). In particular, the somatostatin receptor 3 (SSTR3) is widely expressed in the brain, and is commonly employed as a marker for neuronal cilia (Berbari et al., 2007; Guadiana et al., 2016; Handel et al., 1999; Schulz et al., 2000; Stanic et al., 2009). Moreover, its endogenous ligand somatostatin is expressed by a subset of cortical interneurons

(Gonchar et al., 2007; Lee et al., 2010; Xu et al., 2010). However, the role of somatostatin and SSTR3-mediated signaling in the neocortex is largely uncharacterized.

Expression of SSTR3 begins at birth and increases during postnatal development in the rat hippocampus (Stanic et al., 2009). To begin to examine a possible role for ciliary SSTR3 mediated signaling in regulating excitatory synapses in the cortex, we first characterized the expression and localization of this receptor in primary visual cortex *in vivo.* P15-16 animals were injected with a GFP-expressing AAV viral vector, and 7 days later, brain slices were examined via immunostaining. GFP-expressing pyramidal neurons were identified by their characteristic morphologies, and primary cilia were co-labeled with antibodies against AC3 and SSTR3. We found that the majority of pyramidal neurons across layers contained cilia positive for both AC3 and SSTR3, with a small subset of cilia expressing AC3 alone (Figure 5A,B). In contrast, the majority of GAD67+ neurons expressed AC3 but not SSTR3 (Figure 5C); SSTR3-positive cilia were observed in only a small subset (<10%) of GAD67+ cells that were distributed across layers (Figure 5D). We observed only rare ciliary SSTR3 expression in inhibitory interneurons immunostained with antibodies against the subtype-specific markers choline acetyltransferase (ChAT), parvalbumin (PV) and somatostatin (SOM) (Figure 5D, Figure 5- figure supplement 1), suggesting that the small number of SSTR3-positive GABAergic neurons are likely to be an alternate inhibitory neuron subtype(s).

We next examined SSTR3 expression and localization in cultured cortical neurons. We noted that ~30% of ARL13B-positive cilia on cultured neurons were also positive for SSTR3 at DIV11 as assessed via immunostaining (Figure 5E,F), indicating that SSTR3 is expressed at detectable levels in a subset of these young neocortical neurons. The majority of SSTR3-expressing neurons in culture were excitatory, based on the absence of co-staining with the

inhibitory neuron-specific marker GAD67 (Figure 5E,F). Importantly, SSTR3 was specifically localized to cilia in all expressing cells (Figure 5E). Taken together, these results indicate SSTR3 is expressed primarily, if not exclusively, by excitatory neurons in the neocortex, and is localized specifically to their cilia both *in vitro* and *in vivo*.

Ciliary SSTR3 signaling bidirectionally modulates excitatory synapses in culture

Given that SSTR3 is enriched in the cilia of cortical pyramidal neurons, and somatostatin is present in, and released by, a subset of inhibitory GABAergic interneurons (Gonchar et al., 2007; Lee et al., 2010; Xu et al., 2010), we examined whether signaling via SSTR3 mediates cilia-dependent modulation of excitatory synapse strength. To manipulate SSTR3 signaling, we took advantage of the previously described SSTR3-selective agonist (L-796,778) and antagonist (MK-4256), which can bidirectionally regulate SSTR3-mediated signaling (He et al., 2012; Rohrer et al., 1998; Rohrer and Schaeffer, 2000) (see Methods). We treated DIV10-11 neuronal cultures for varying periods of time with either the agonist or antagonist, and then fixed and stained for excitatory pre- and post-synaptic markers. Since not all pyramidal neurons in culture express detectable SSTR3 in their cilia, we additionally immunostained with antibodies against SSTR3, and confined our analysis to neurons with robust SSTR3 expression. Because of species overlap between antibodies, we used Shank3 as the postsynaptic marker for these experiments; Shank3 specifically localizes to excitatory synapses and the intensity of synaptic Shank3 is correlated with postsynaptic strength (Monteiro and Feng, 2017; Tatavarty et al., 2020; Verpelli et al., 2011).

Manipulating SSTR3 signaling induced bidirectional changes in the intensity of both Shank3 and VGlut1 at colocalized sites, that developed over several hours (Figure 6A,B, Figure

6 – figure supplement 1A). The SSTR3 antagonist significantly increased synaptic Shank3 (Figure 6A,B), and VGlut1 intensity (Figure 6 – figure supplement 1A), while the SSTR3 agonist significantly reduced the fluorescence intensities of both markers (Figure 6A,B, Figure 6 – figure supplement 1A). The SSTR3 agonist also significantly reduced the density of putative excitatory synapses, while the effects of the antagonist on synapse density did not reach statistical significance (Figure 6C). Experiments were performed using the lowest concentrations of each compound at which synaptic effects were observed (Figure 6 – figure supplement 1B,C). Taking advantage of the temporal resolution of these pharmacological experiments, we determined how rapidly these manipulations were able to modulate synaptic properties. We found that the first detectable effects were evident after 18 hr and were more robust after 24 hrs of treatment (Figure 6B,C). Neither the agonist nor the antagonist altered cilia lengths (Figure 6 – figure supplement 1D) or affected cell viability (Figure 6 – figure supplement 1E). These results indicate that SSTR3-mediated signaling through cilia can dynamically regulate excitatory synaptic properties, and suggest that activation of SSTR3 receptors by exogenous ligands may be able to negatively regulate excitatory synaptic strength.

DISCUSSION

We show here that cilia play a critical role in the maintenance of neuronal excitability in the postnatal cortex. Acute disruption of ciliary signaling cell-autonomously and rapidly strengthens excitatory synapses onto pyramidal glutamatergic neurons, without affecting inhibitory synapses. Consequently, neurons with disrupted cilia have more and stronger excitatory synapses, and increased spontaneous firing rates. We find that the SSTR3 neuropeptide receptor is selectively localized to the cilia of cortical pyramidal neurons, and that

inhibition or activation of SSTR3-mediated signaling bidirectionally modulates excitatory synapses onto these neurons on similar rapid hours-long timescales. Our results indicate that neuropeptidergic signaling via cilia-localized receptors can dynamically modulate neuronal excitability, and raise the possibility that disorders arising from altered E/I balance in cortical circuits may in part be due to defects in cilia function in the postnatal mammalian brain.

We find that acute and cell-autonomous cilia perturbation affects excitatory synapses onto pyramidal neurons, without impacting dendritic inhibitory synapse number, dendritic arborization, intrinsic neuronal excitability, or passive neuronal properties. Thus, this rapid ciliary signaling pathway appears to be specific for the regulation of excitatory synapses. However, there are many neocortical inhibitory interneuron types that synapse onto specific postsynaptic domains of pyramidal neurons (Kepecs and Fishell, 2014; Tremblay et al., 2016; Urban-Ciecko and Barth, 2016), and our data do not rule out the possibility that some classes of inhibitory synapses may also be affected. Nevertheless, the net impact of the observed synaptic changes leads to increased firing rates, suggesting that any effects on inhibition also contribute to this enhanced excitability, or are not sufficient to counteract changes in excitatory synaptic drive. It is also currently unknown whether ciliary signaling in neocortical GABAergic interneurons similarly rapidly modulates their synaptic or intrinsic properties. We speculate that cell type-specific ciliary signaling pathways that integrate distinct extracellular cues may also have important roles in neocortical interneuron subtypes. In this work, we describe the direct and cell-autonomous impact of ciliary signaling in pyramidal neurons. It is likely that the circuit-level impact on excitatory and inhibitory synaptic loops, and thus on circuit excitability, will be more complex in ciliopathies that affect cilia function in all neocortical cell types.

SSTR3 is selectively enriched in the cilia of pyramidal neurons, with rare expression in inhibitory neuron cilia. SOM+ interneurons are present throughout cortical layers (Urban-Ciecko and Barth, 2016), suggesting that these interneurons may modulate excitatory neurons via cilia localized SSTR3. Since AC3 is present in the cilia of both excitatory and inhibitory neurons, inhibitory neuron cilia are likely to contain a distinct complement of signaling proteins. Neuronal cilia in the brain express Sonic hedgehog (Shh) signaling components, dopamine and serotonin receptor subtypes, as well as subsets of neuropeptide and neurohormone receptors in a brain region- and cell type-specific manner (Berbari et al., 2008b; Brailov et al., 2000; Domire et al., 2011; Green et al., 2012; Hamon et al., 1999; Handel et al., 1999; Koemeter-Cox et al., 2014; Loktev and Jackson, 2013; Sipos et al., 2018). Adding to this complexity, ciliary localization of these molecules can be dynamically modulated by extracellular signals (Bangs and Anderson, 2017; Domire et al., 2011; Green et al., 2016; Nachury, 2018; Najafi and Calvert, 2012). Thus, as in olfactory neurons and photoreceptors, central neurons likely actively regulate the targeting and localization of ciliary signal transduction proteins as a function of cell type, developmental stage, and context. This dynamic control of cilia signaling protein content in turn likely allows these organelles to appropriately sense changing extracellular cues, and transduce these cues to regulate diverse aspects of neuronal development and function.

There is now increasing evidence of a link between cilia and the establishment and maintenance of synapses in the brain. Prolonged loss of cilia results in loss of synapses with associated changes in dendritic complexity in multiple brain regions (Bowie and Goetz, 2020; Guo et al., 2017; Kumamoto et al., 2012), and we find that acute loss of ciliary signaling rapidly alters excitatory synaptic properties without any apparent effects on dendritic morphology. Overexpression of cilia-targeted SSTR3 in Arl13b-deficient interneurons restores interneuron

morphology and connectivity (Guo et al., 2017), suggesting that signaling via SSTR3 is sufficient to maintain these inhibitory networks. In cultured cortical neurons, we find that acute ARL13B knockdown phenocopies the effects of SSTR3 antagonism on excitatory synapses, implying that ciliary SSTR3 negatively regulates excitatory synapse strength. How might neuropeptidergic signaling from a cilium located on the soma be transmitted to regulate different aspects of synaptic function on different timescales? Ciliary GPCRs couple to multiple cilia-localized effectors to alter levels of second messengers such as cAMP, calcium and PI(3,4,5)P3 (Bielas et al., 2009; Delling et al., 2013; Garcia-Gonzalo et al., 2015; Green and Mykytyn, 2014; Guo et al., 2019; Hansen et al., 2020; Hilgendorf et al., 2016; Humbert et al., 2012; Moore et al., 2016; Mukherjee et al., 2016; Mukhopadhyay et al., 2013; Mykytyn and Askwith, 2017; Schou et al., 2015; Su et al., 2013). These ciliary signals can propagate throughout the cell by as yet unknown mechanisms and activate diverse downstream molecules including the AKT and PKA kinases, as well as transcription factors such as CREB (Anvarian et al., 2019; Bielas et al., 2009; Guo et al., 2019; Manning and Toker, 2017; Mick et al., 2015; Moore et al., 2016; Mukhopadhyay et al., 2013; Plotnikova et al., 2015; Tuson et al., 2011). A role for calcium-, cAMP- and CREB-mediated changes in gene expression that contribute to some forms of activity-dependent synaptic plasticity is well-established (Flavell and Greenberg, 2008; Heinz and Bloodgood, 2020; West and Greenberg, 2011; Yap and Greenberg, 2018). Similar transcription-dependent mechanisms may also underlie cilia-driven regulation of network connectivity. On more rapid timescales, ciliary signaling may modulate synaptic strength via posttranslational regulation of synaptic protein function. For instance, cAMP- and calcium-dependent kinases such as PKA and CaMKII modulate synaptic plasticity via direct phosphorylation of AMPA receptor subunits (Buonarati et al., 2019; Herring and Nicoll, 2016);

the functions of one or both these kinases at synapses could be modulated by signals from cilia. An important goal for the future will be to identify the ciliary mechanisms and pathways that operate on distinct timescales to modulate synapse establishment, maintenance, and plasticity.

Altered E/I balance in central circuits is linked to a wide range of neurodevelopmental disorders and neuropsychiatric diseases (Hoftman et al., 2017; Nelson and Valakh, 2015; Sohal and Rubenstein, 2019). Intriguingly, many ciliopathies are also characterized by neurological deficits, and altered cilia function and ciliary signaling is associated with defects in neuronal plasticity and circuit functions (Bennouna-Greene et al., 2011; Berbari et al., 2014; Cantagrel et al., 2008; Chen et al., 2016; Einstein et al., 2010; Guemez-Gamboa et al., 2014; Marley and von Zastrow, 2012; Rhee et al., 2016; Wang et al., 2011; Yao et al., 2016). Moreover, association and linkage studies have identified ciliary genes associated with schizophrenia, autism spectrum disorder, major depressive disorder, bipolar disorder and others (Chubb et al., 2008; Karunakaran et al., 2020; O'Donovan et al., 2008; RK et al., 2017; Torri et al., 2010; Wray et al., 2012). Our findings raise the possibility that defects in continuous maintenance of E/I balance by ciliary signaling may underlie a subset of behavioral and cognitive dysfunction linked with mental disorders. These observations establish the cilium as a major modulator of circuit homeostasis in postnatal neurons, and highlight the critical importance of future studies of the signaling mechanisms by which this organelle regulates neuronal functions in development and disease.

METHODS

All experimental procedures were approved by the Brandeis IACUC and were performed according to NIH guidelines. All data files used to generate each figure are included as Source Data Files.

Dissociated cortical neuron cultures and transfection

Dissociated cortical neuron cultures were prepared from visual cortices of male or female P0-3 Long-Evans rat pups and plated on confluent astrocytes as described previously (Pratt et al., 2003). Sparse transfections of plasmid DNA were performed after DIV9-10 with Lipofectamine 2000 (Thermo Fisher). GFP-expressing pyramidal neurons were identified by their characteristic morphologies and used for imaging or recording after either 24 or 48 hrs. Dissociation-matched sister cultures were transfected with vectors expressing GFP alone as controls. All experiments were replicated a minimum of 3 times from independent dissociations. Data acquisition and analyses were performed blind to treatment conditions.

Immunofluorescent staining

Cells from DIV11 cultures were fixed with 4% PFA/ 5% sucrose for 5 or 15 minutes, and permeabilized with either ice cold methanol for 10 minutes, or 0.2% Triton X-100 for 5 minutes. Primary antibodies were applied for either 1 hr at room temperature or overnight at 4°C. To detect GluA2 at the cell membrane, immunostaining was performed prior to permeabilizing. Primary antibodies included: αARL13B [1:1000, NeuroMab N295B/66 (75-287)], αIFT88 (1:500, Millipore ABC932), αAC3 (1:500, EnCor RPCA-ACIII, MCA-1A12), αSSTR3 (1:2000, Biotrend-USA SS-830-50), αGluA2 (1:1000, gift from Gouaux lab, OHSU), αVGlut1 (1:1000,

Synaptic Systems 135 304, 135 316), αShank3 (1:1000, Synaptic Systems 162 304), αPV (1:500, Synaptic Systems 195 011), αSOM (1:500, Thermo Fisher 14-9751-82), αChAT (1:100, Millipore AB144P), αGAD67 (1:2000, Millipore MAB5406; 1:2000, R&D Systems AF2086). Secondary antibodies (Thermo Fisher) were incubated for 1-4 hrs at room temperature. Slides were mounted using Fluoromount-G.

Vectors and shRNAs

shRNA sequences were designed with the TRC algorithm (Broad Institute). Vectors used are listed in Table S1. The pLKO.1 TRC cloning vector was a gift from David Root (RRID: Addgene_10878) (Moffat et al., 2006), the AAV-shRNA-ctrl was a gift from Hongjun Song (RRID: Addgene_85741) (Yu et al., 2015), the pAAV-hSyn-EGFP and viral prep 50465-AAV9 was a gift from Bryan Roth (RRID: Addgene_50465). Annealed oligos for shCep164 (5'-CAACAACCACATCGAACTTA-3'), shIft88 (5'-CGAATGGCTTGGAGCTTATTA-3'), and shArl13b_2 (5'-GCTCAGGACATGATCTCATAA), were cloned into modified pAAV-shRNA-ctrl or pSUPER vectors (Oligoengine). The sequence of shArl13b_1 was modified from a previously validated shArl13b sequence (5'-CCTGTCAGAAAGGTGACACTT-3') (Larkins et al., 2011), and cloned into pLKO.1 and modified pAAV-shRNA-ctrl vectors using Gibson cloning.

Microscopy and image analysis

Immunostained cells and brain sections were mounted on slides and imaged on either a Zeiss LSM 880 confocal or Zeiss LSM 880 with Airyscan confocal microscope using Plan-Apochromat 63x/1.40 oil objectives. Cilia were labeled with two markers and fluorescence

intensity was quantified from ROIs using either Metamorph (Molecular Devices) or ImageJ (NIH). Background fluorescence was subtracted using ROIs from the cell soma or from regions without neurons. Total fluorescence per ROI was averaged and normalized to control treatments. Quantification of synaptic protein intensity and synapse density was performed similar to our published procedures (Gainey et al., 2015; Tatavarty et al., 2020). Images were taken distal to the primary branch point of apical-like dendrites to ensure uniformity across samples. Analyses of synaptic protein intensity were performed using the Granularity application module in Metamorph; granules with a minimum overlap of 3 pixels in all channels were defined as colocalized puncta and selected for analysis. Total pixel intensities of each punctum were summed and then averaged across puncta for each neuron. For quantification of dendritic complexity, tiled images of apical-like arbors were taken and lengths were measured using ImageJ (NIH); nodes were counted at primary, secondary and tertiary branch points.

Electrophysiology

Whole cell patch clamp experiments were performed using an Axopatch 200B amplifier (Molecular Devices) on an Olympus IX70 inverted microscope equipped with differential interference contrast optics and epifluorescence. Recordings were performed at room temperature with an internal solution containing: 120 mM $KMeSO_4$, 10 mM KCl, 2 mM $MgSO_4$, 0.5 mM EGTA, 10 mM HEPES, 3 mM K_2ATP, 0.3 mM NaGTP, 10 mM Na_2 phosphocreatine; dextrose was used to adjust osmolarity to 320-330 mOsm. Cultures were superfused with artificial cerebral spinal fluid (aCSF) containing: 1 mM NaH_2PO_4, 25 mM $NaHCO_3$, 126 mM NaCl, 5.5 mM KCl, 2 mM $MgSO_4$, 2 mM $CaCl_2$; dextrose was used to adjust osmolarity to 330-340 mOsm. GFP-expressing pyramidal neurons were identified by their characteristic

morphologies. Neurons with V_m > -50 mV, R_s >20 MΩ, R_{in} <100 MΩ, or with V_m or R_{in} changed by ≥10% during the recording were excluded from analysis.

Spontaneous firing rates: Spontaneous firing rates were recorded in whole cell current clamp mode. A small DC current was injected to keep the resting potential near -55 mV. 10 sweeps of 20 sec each were obtained for each neuron and average firing rate was calculated for the entire period of the recording. Spikes were detected automatically using a threshold crossing function written in R (https://github.com/latereshko/current_clamp_scripts).

Instantaneous firing rates: F/I recordings were made in whole cell current clamp using depolarizing current steps between 10-400 pA in aCSF containing 25 μM picrotoxin, 50 μM APV and 25 μM DNQX to block synaptic currents. Recordings were acquired with Igor Pro (WaveMetric) and analyzed as described using custom scripts in MATLAB (MathWorks) (Joseph and Turrigiano, 2017). Instantaneous firing rate was calculated as the reciprocal of the interval of the first two consecutive spikes (https://github.com/latereshko/current_clamp_scripts).

mEPSC recordings: Whole cell voltage clamp recordings were obtained from neurons held at -70 mV. AMPAR-mediated currents were isolated by adding 25 μM picrotoxin, 25 μM APV, and 0.1 μM TTX to aCSF. Events that were <5 pA in amplitude, or <3 ms in rise time were excluded from analysis. Recordings were analyzed as described using custom scripts in IGOR Pro (Joseph and Turrigiano, 2017; Tatavarty et al., 2020) (https://github.com/latereshko/mEPSC_scripts).

SSTR3 Pharmacology

The antagonist MK-4256 was purchased from MedChemExpress (HY-13466). The agonist L-796,778 was a generous gift from Merck Pharmaceuticals and was purified via HPLC

to isolate the active compound from degraded material (Isaac Krauss, Brandeis University). Compounds were dissolved in DMSO to make 1 mM stock concentrations. DIV10-11 cultures were treated with 0.125 μM, 0.5 μM, 1 μM or 2 μM concentrations of either reagent for the indicated time periods of 6 hrs, 18 hrs, or 24 hrs. Cells were fixed, immunostained, and imaged as described above.

AAV viral injections

Virus were diluted in bacteriostatic 0.9% saline on the day of injection (on ice). Prior to surgeries, animals were anesthetized with isoflurane (1.0-2.0% concentration in air) delivered by a SomnoSuite anesthesia system with integrated digital vaporizer (Kent Scientific) through a stereotaxic head holder. Primary visual cortex was bilaterally targeted using stereotaxic coordinates for lambda-bregma distances according to age (P15-16). After craniotomy was performed over the targeted area, a glass micropipette was lowered into the brain and delivered 800 nL of virus-containing solution at the targeted depth. Control and shRNA expressing virus were injected in different hemispheres. Animals were monitored in separate cages for 12-24 hrs post-injection.

Transcardial perfusions and slices preparation

After 7 days of virus expression, animals (P22-23) were deeply anesthetized with heavy dosage of ketamine/xylazine/acepromazine (KXA) cocktail (140 mg/kg ketamine; 7 mg/kg xylazine; 1.4 mg/kg acepromazine) and perfused with 5 ml 1X phosphate-buffered saline (PBS) followed by 10-15 ml of 4% paraformaldehyde (PFA) in PBS at room temperature. The brain was removed and preserved in a solution of 4% PFA overnight. After incubation, brain tissues

went through three 10 min washes of 1X PBS. Brain tissue was sectioned preserving visual cortex and mounted onto the vibratome with super glue. 50-75 µm sections were collected in a PBS-containing well. Free floating sections were immunostained as described above.

Cell viability

Cell viability was assessed by co-staining with propidium iodide (Thermo Fisher P3566) and the amine-reactive fluorescent dye Zombie Green (BioLegend 423111). Zombie Green was reconstituted in 100 µl of DMSO. Cultures of neurons were incubated with 50 µg/mL propidium iodide and 1:1000 diluted Zombie Green 10 mins before fixation. Cells were fixed as described above. Cells were imaged by confocal microscopy as described above and scored as dead when positively stained for either or both propidium iodide and Zombie Green.

Statistical analysis

All experiments were replicated a minimum of 3 times from biologically independent dissociations performed on different days. Data acquisition and analyses were performed blind to treatment conditions. R software (version 4.0.3) and R Studio were used for statistical analyses (https://www.R-project.org/ and http://www.rstudio.com/). Plots were generated using the package ggplot2 (v3.3.2) (https://cran.r-project.org/web/packages/ggplot2/). Wilcoxon rank-sum or Kruskal-Wallis tests with Dunn's posthoc test for multiple comparisons were used to compare non-normal distributions (dunn.test v1.3.5) (https://CRAN.R-project.org/package=dunn.test). For synaptic protein intensity analyses, values of experimental samples were normalized to the mean values of the control group for each experiment, and linear mixed models (LMM) were used in place of ANOVA to address the non-independence of measurements taken from the same

experimental animal or dissociation, using the lme4 package (v1.1-25) (https://cran.r-project.org/web/packages/lme4/). Comparisons were made using random intercept terms for experimental replicate and culture dish, to address variability between preparations and the non-independence of cells imaged from the same dishes. P-values were approximated using the Kenward-Roger method and adjusted with Dunnett's post hoc correction as implemented by the emmeans package (v1.5.2-1) (https://CRAN.R-project.org/package=emmeans). Statistical tests used, P-values, and sample and replicate numbers for each figure are summarized in Table S2. All data and analysis codes can be found at (https://github.com/latereshko/Tereshko_neuron_cilia)

Acknowledgements

We thank Vedakumar Tatavarty for experimental assistance, Kim McDermott and Greg Pazour for advice regarding knockdown of ciliary proteins, and Mike O'Donnell for advice and assistance with R and statistical analyses. We are grateful to Merck for the gift of L-796,778 and to Isaac Krauss for purification of this chemical. We thank the Sengupta and Turrigiano labs for input and advice. This work was funded by the NIH grants R35 GM122463 (P.S.), R21 MH118464 (P.S. and G.G.T), and R35NS111562 (G.G.T.).

FIGURE LEGENDS

Figure 1. Acute knockdown of ciliary proteins does not alter dendritic morphology of cortical pyramidal neurons.

A) Representative images of a DIV11 pyramidal neuron expressing GFP (top), and an inhibitory neuron immunolabeled with GAD67 antibodies (bottom). Cilia (arrows) are immunolabeled using antibodies against AC3 and ARL13B (top) or ARL13B alone (bottom). Scale bars: 5 µm.

B) Percentage of inhibitory (GAD67+) and excitatory (GAD67-) neurons containing cilia immunolabeled with antibodies against AC3 and/or ARL13B. n = 150 total; 3 dissociations.

C) Lengths of cilia in excitatory and inhibitory neurons. Each dot is a measurement from a single neuron. Bars are average ± SEM. n: GAD67+ = 44, GAD67- = 46; 5 dissociations.

D) Representative images of neurons expressing GFP alone (top) or shArl13b_1 and GFP (see Table S1) (bottom). Cilia were immunolabeled with antibodies against AC3 and ARL13B. Images at right show enlarged (2.5X) views of cilia (yellow boxes). Scale bars: 5 µm.

E, F) Relative fluorescence intensities of immunolabeled ciliary ARL13B **(E)**, and cilia lengths **(F)**, in neurons transfected with the indicated plasmids. Each dot is a measurement from a single neuron. Values in **E** are normalized to intensity in control neurons. Bars are average ± SEM. *** indicates P<0.001 for the indicated conditions (Kruskal-Wallis with Dunn's multiple comparisons test). n: Control = 34, shArl13b_1 = 43, shArl13b_2 = 40; 4 dissociations.

G) Representative images of pyramidal neurons expressing GFP alone (control) or shArl13b_1 and GFP. Scale bar: 50 µm.

H, I) Total lengths **(H)** and number of branch points **(I)** of apical-like dendritic arbors of neurons expressing GFP or shArl13b_1 and GFP. Each dot is a measurement from a single neuron. Bars are average ± SEM. n: Control = 32, shArl13b_1 = 28; 4 dissociations.

Here and below, statistical tests used and exact p values for each comparison are shown in Table S2.

Also see Figure 1 – figure supplement 1.

Figure 2. Acute knockdown of ciliary proteins increases the strength and number of excitatory synapses.

A, B, E) Representative images of pyramidal neuron dendrites immunolabeled with antibodies against GluA2 and VGlut1 **(A, B)**, or Gephyrin and GAD65 **(E)**. Cultures were transfected with GFP alone or together with the indicated plasmids. Scale bars: 5 μm.

C) Relative fluorescence intensity of immunolabeled GluA2 at GluA2 /VGlut1 colocalized puncta for indicated conditions at 24 hrs or 48 hrs following transfection. Intensity values are normalized to controls. Each dot is the average summed pixel value for all measured synapses from a given neuron. Bars are average ± SEM. ** and *** indicate P<0.01 and 0.001, respectively, for the indicated conditions (LMM with Dunnett-type correction for multiple comparisons). n: Control = 25 (24 hrs) and 32 (48 hrs), shArl13b_1 = 24, shArl13b_2 = 19, shIft88/shCep164 = 39; 4 dissociations.

D) Number of colocalized GluA2/VGlut1 puncta per μm of dendrite analyzed (density) onto neurons transfected with the indicated plasmids at 24 hrs or 48 hrs following transfection. Each dot is the density of synapses examined per neuron. Bars are average ± SEM. * indicates P<0.05 for the indicated conditions (LMM with Dunnett-type correction for multiple comparisons); additional P-values are also indicated. n: As in **C.**

F) Relative fluorescence intensity of immunolabeled Gephyrin at colocalized puncta on neurons transfected with the indicated plasmids at 24 hrs following transfection. Intensity values are

normalized to values in control neurons. Each dot is the average summed pixel value for all measured synapses from a given neuron. Bars are average ± SEM. n: Control = 17, shArl13b_1 = 22 neurons; 4 dissociations.

G) Number of colocalized Gephryin/GAD65 puncta per μm of dendrite analyzed (density) onto neurons transfected with the indicated plasmids at 24 hrs following transfection. Each dot is the density of synapses examined per neuron. Bars are average ± SEM. n: As in **F**.

Also see Figure 2 – figure supplement 1.

Figure 3. Mean mEPSC amplitude in pyramidal neurons is increased following acute reduction of ciliary signaling.

A) (Left) Representative mEPSC traces (top) and average waveforms (bottom) from neurons transfected with the indicated plasmids. (Right) mEPSC amplitude from neurons transfected with the indicated plasmids. Each dot represents the average amplitude for a given neuron. Bars are average ± SEM. ** indicate different between indicated values at $P<0.01$ (Kruskal-Wallis with Dunn's multiple comparisons test). n: Control = 24, shArl13b_1 = 24, shArl13b_2 = 23; >5 dissociations.

B, C) Cumulative distribution probabilities of mEPSC amplitudes **(B)** and inter-event intervals **(C)** from neurons transfected with the indicated plasmids. *** indicates different from control at $P<0.001$ (Kruskal-Wallis with Bonferroni correction).

D, E) Average resting membrane potential (V_m) **(D)** and input resistance (R_{in}) **(E)** of neurons transfected with the indicated plasmids. Each dot represents a single neuron. Bars are average ± SEM. n: As in **A**.

Figure 4. Disruption of ciliary signaling increases spontaneous firing without influencing intrinsic excitability.

A) (Left) Representative voltage traces of spontaneous activity recorded from pyramidal neurons expressing GFP alone or shArl13b_1 and GFP. (Right) Average spontaneous firing rate for neurons transfected with the indicated plasmids. Each dot represents one neuron. Bars are average ± SEM. * indicates different between indicated values at $P<0.05$ (Wilcoxon rank-sum test). n: Control = 32, shArl13b_1 = 25; >5 dissociations.

B) (Left) Representative responses of pyramidal neurons expressing GFP or shArl13b_1 and GFP during current injection. (Right) Average instantaneous firing rate vs current curves for neuron transfected with the indicated plasmids. Errors are SEM. n: Control =18, shArl13b_1 = 20; 3 dissociations.

Figure 5. SSTR3 is localized to the cilia of excitatory, but not inhibitory, cortical neurons.

A) Representative images of primary cilia immunolabeled with antibodies against AC3 and SSTR3 in GFP-expressing neurons in fixed cortical slices from P22 animals. Images at right show enlarged (2.5X) views of cilium (yellow box; arrow). Scale bars: 5 µm.

B) Percentage of GFP-expressing pyramidal neurons with primary cilia co-expressing AC3 and SSTR3 categorized by cortical layer. n=150 neurons per layer; 3 animals.

C) Representative images of a GAD67-expressing inhibitory neuron in fixed cortical tissue stained with DAPI. Cilia were immunolabeled with antibodies against AC3 and SSTR3. The cilium is indicated with an arrow. Scale bar: 5 µm.

D) Percentage of inhibitory neurons of the indicated subtype containing SSTR3+ primary cilia in fixed cortical tissue. Cilia were identified via co-immunostaining with anti-AC3 or anti-PCTN

antibodies. n: Excitatory =150, GAD67+ = 115, ChAT+ = 31, PV+ = 100, SOM+ = 110; 3 dissociations.

E) Representative images of cultured neurons immunolabeled with antibodies against GAD67, ARL13B and SSTR3, and co-stained with DAPI. Arrows indicate cilia of GAD- (top) and GAD+ (bottom) neurons. Scale bars; 5 μm.

F) Quantification of cultured neurons immunolabeled with antibodies against GAD67, ARL13B and SSTR3. n = 515 total; 4 dissociations.

Also see Figure 5 – figure supplement 1.

Figure 6. Pharmacological modulation of SSTR3 bidirectionally regulates excitatory synapses.

A) Representative images of pyramidal neuron dendrites immunolabeled with antibodies against Shank3 (Shk3) and VGlut1. Cultures were treated for 24 hrs with 2 μM L-796,798 (SSTR3 agonist) or 1 μM MK-4256 (SSTR3 antagonist) prior to staining. Scale bars: 5 μm.

B) Relative fluorescence intensity of Shk3 at colocalized Shk3/VGlut1 puncta on neurons treated with the indicated compounds and fixed and immunostained 6, 18, or 24 hrs after addition of drug. Intensity values are normalized to values in control neurons. Each dot is the average summed pixel value of all examined synapses per neuron. Bars are average ± SEM. ** and *** indicate P<0.01 and 0.001, respectively for the indicated conditions (LMM with Dunnett-type correction for multiple comparisons); additional P-values are also shown. n: (6 hrs) Control = 23, agonist = 10, antagonist = 17; (18 hrs) Control = 35, agonist = 33, antagonist = 17; (24 hrs) Control = 87, agonist = 17, antagonist =40; ≥3 dissociations.

C) Number of colocalized Shk3/VGlut1 puncta per μm of dendrite analyzed (density) onto neurons treated with the indicated compounds. Cultures were immunostained at the indicated

times following addition of the compounds. Each dot is the density of synapses examined per neuron. Bars are average ± SEM. * indicates $P<0.05$ for the indicated conditions (LMM with Dunnett-type correction for multiple comparisons). n: as in **B.**

Also see Figure 6 – figure supplement 1.

REFERENCES

Anvarian, Z., Mykytyn, K., Mukhopadhyay, S., Pedersen, L.B., and Christensen, S.T. (2019). Cellular signalling by primary cilia in development, organ function and disease. Nat Rev Nephrol *15*, 199-219.

Arellano, J.I., Guadiana, S.M., Breunig, J.J., Rakic, P., and Sarkisian, M.R. (2012). Development and distribution of neuronal cilia in mouse neocortex. J Comp Neurol *520*, 848-873.

Bangs, F., and Anderson, K.V. (2017). Primary cilia and mammalian hedgehog signaling. Cold Spring Harb Perspect Biol *9*, a028175.

Baudoin, J.P., Viou, L., Launay, P.S., Luccardini, C., Espeso Gil, S., Kiyasova, V., Irinopoulou, T., Alvarez, C., Rio, J.P., Boudier, T.*, et al.* (2012). Tangentially migrating neurons assemble a primary cilium that promotes their reorientation to the cortical plate. Neuron *76*, 1108-1122.

Bennouna-Greene, V., Kremer, S., Stoetzel, C., Christmann, D., Schuster, C., Durand, M., Verloes, A., Sigaudy, S., Holder-Espinasse, M., Godet, J.*, et al.* (2011). Hippocampal dysgenesis and variable neuropsychiatric phenotypes in patients with Bardet-Biedl syndrome underline complex CNS impact of primary cilia. Clin Genet *80*, 523-531.

Berbari, N.F., Bishop, G.A., Askwith, C.C., Lewis, J.S., and Mykytyn, K. (2007). Hippocampal neurons possess primary cilia in culture. J Neurosci Res *85*, 1095-1100.

Berbari, N.F., Johnson, A.D., Lewis, J.S., Askwith, C.C., and Mykytyn, K. (2008a). Identification of ciliary localization sequences within the third intracellular loop of G protein-coupled receptors. Mol Biol Cell *19*, 1540-1547.

Berbari, N.F., Lewis, J.S., Bishop, G.A., Askwith, C.C., and Mykytyn, K. (2008b). Bardet-Biedl syndrome proteins are required for the localization of G protein-coupled receptors to primary cilia. Proc Natl Acad Sci USA *105*, 4242-4246.

Berbari, N.F., Malarkey, E.B., Yazdi, S.M., McNair, A.D., Kippe, J.M., Croyle, M.J., Kraft, T.W., and Yoder, B.K. (2014). Hippocampal and cortical primary cilia are required for aversive memory in mice. PLoS One *9*, e106576.

Bielas, S.L., Silhavy, J.L., Brancati, F., Kisseleva, M.V., Al-Gazali, L., Sztriha, L., Bayoumi, R.A., Zaki, M.S., Abdel-Aleem, A., Rosti, R.O.*, et al.* (2009). Mutations in INPP5E, encoding inositol polyphosphate-5-phosphatase E, link phosphatidyl inositol signaling to the ciliopathies. Nat Genet *41*, 1032-1036.

Bishop, G.A., Berbari, N.F., Lewis, J., and Mykytyn, K. (2007). Type III adenylyl cyclase localizes to primary cilia throughout the adult mouse brain. J Comp Neurol *505*, 562-571.

Bowie, E., and Goetz, S.C. (2020). TTBK2 and primary cilia are essential for the connectivity and survival of cerebellar Purkinje neurons. Elife *9*, e51166.

Brailov, I., Bancila, M., Brisorgueil, M.J., Miquel, M.C., Hamon, M., and Verge, D. (2000). Localization of 5-HT(6) receptors at the plasma membrane of neuronal cilia in the rat brain. Brain Res *872*, 271-275.

Buonarati, O.R., Hammes, E.A., Watson, J.F., Greger, I.H., and Hell, J.W. (2019). Mechanisms of postsynaptic localization of AMPA-type glutamate receptors and their regulation during long-term potentiation. Sci Signal *12*, eaar6889.

Cantagrel, V., Silhavy, J.L., Bielas, S.L., Swistun, D., Marsh, S.E., Bertrand, J.Y., Audollent, S., Attie-Bitach, T., Holden, K.R., Dobyns, W.B.*, et al.* (2008). Mutations in the cilia gene ARL13B lead to the classical form of Joubert syndrome. Am J Hum Genet *83*, 170-179.

Caspary, T., Larkins, C.E., and Anderson, K.V. (2007). The graded response to Sonic Hedgehog depends on cilia architecture. Dev Cell *12*, 767-778.

Cevik, S., Hori, Y., Kaplan, O.I., Kida, K., Toivenon, T., Foley-Fisher, C., Cottell, D., Katada, T., Kontani, K., and Blacque, O.E. (2010). Joubert syndrome Arl13b functions at ciliary membranes and stabilizes protein transport in *Caenorhabditis elegans*. J Cell Biol *188*, 953-969.

Chen, X., Luo, J., Leng, Y., Yang, Y., Zweifel, L.S., Palmiter, R.D., and Storm, D.R. (2016). Ablation of type III adenylyl cyclase in mice causes reduced neuronal activity, altered sleep pattern, and depression-like phenotypes. Biol Psychiatry *80*, 836-848.

Chizhikov, V.V., Davenport, J., Zhang, Q., Shih, E.K., Cabello, O.A., Fuchs, J.L., Yoder, B.K., and Millen, K.J. (2007). Cilia proteins control cerebellar morphogenesis by promoting expansion of the granule progenitor pool. J Neurosci *27*, 9780-9789.

Chubb, J.E., Bradshaw, N.J., Soares, D.C., Porteous, D.J., and Millar, J.K. (2008). The DISC locus in psychiatric illness. Mol Psychiatry *13*, 36-64.

Davis, E.E., and Katsanis, N. (2012). The ciliopathies: a transitional model into systems biology of human genetic disease. Curr Opin Genet Dev *22*, 290-303.

Delling, M., DeCaen, P.G., Doerner, J.F., Febvay, S., and Clapham, D.E. (2013). Primary cilia are specialized calcium signalling organelles. Nature *504*, 311-314.

Domire, J.S., Green, J.A., Lee, K.G., Johnson, A.D., Askwith, C.C., and Mykytyn, K. (2011). Dopamine receptor 1 localizes to neuronal cilia in a dynamic process that requires the Bardet-Biedl syndrome proteins. Cell Mol Life Sci *68*, 2951-2960.

Einstein, E.B., Patterson, C.A., Hon, B.J., Regan, K.A., Reddi, J., Melnikoff, D.E., Mateer, M.J., Schulz, S., Johnson, B.N., and Tallent, M.K. (2010). Somatostatin signaling in neuronal cilia is critical for object recognition memory. J Neurosci *30*, 4306-4314.

Elliott, K.H., and Brugmann, S.A. (2019). Sending mixed signals: Cilia-dependent signaling during development and disease. Dev Biol *447*, 28-41.

Flavell, S.W., and Greenberg, M.E. (2008). Signaling mechanisms linking neuronal activity to gene expression and plasticity of the nervous system. Annu Rev Neurosci *31*, 563-590.

Gainey, M.A., Tatavarty, V., Nahmani, M., Lin, H., and Turrigiano, G.G. (2015). Activity-dependent synaptic GRIP1 accumulation drives synaptic scaling up in response to action potential blockade. Proc Natl Acad Sci USA *112*, E3590-3599.

Garcia-Gonzalo, F.R., Phua, S.C., Roberson, E.C., Garcia, G., 3rd, Abedin, M., Schurmans, S., Inoue, T., and Reiter, J.F. (2015). Phosphoinositides regulate ciliary protein trafficking to modulate Hedgehog signaling. Dev Cell *34*, 400-409.

Gerdes, J.M., Davis, E.E., and Katsanis, N. (2009). The vertebrate primary cilium in development, homeostasis, and disease. Cell *137*, 32-45.

Goetz, S.C., and Anderson, K.V. (2010). The primary cilium: a signalling centre during vertebrate development. Nat Rev Genet *11*, 331-344.

Gonchar, Y., Wang, Q., and Burkhalter, A. (2007). Multiple distinct subtypes of GABAergic neurons in mouse visual cortex identified by triple immunostaining. Front Neuroanat *1*, 3.

Graser, S., Stierhof, Y.D., Lavoie, S.B., Gassner, O.S., Lamla, S., Le Clech, M., and Nigg, E.A. (2007). Cep164, a novel centriole appendage protein required for primary cilium formation. J Cell Biol *179*, 321-330.

Green, J.A., Gu, C., and Mykytyn, K. (2012). Heteromerization of ciliary G protein-coupled receptors in the mouse brain. PLoS One *7*, e46304.

Green, J.A., and Mykytyn, K. (2014). Neuronal primary cilia: an underappreciated signaling and sensory organelle in the brain. Neuropsychopharmacology *39*, 244-245.

Green, J.A., Schmid, C.L., Bley, E., Monsma, P.C., Brown, A., Bohn, L.M., and Mykytyn, K. (2016). Recruitment of beta-Arrestin into neuronal cilia modulates somatostatin receptor subtype 3 ciliary localization. Mol Cell Biol *36*, 223-235.

Guadiana, S.M., Parker, A.K., Filho, G.F., Sequeira, A., Semple-Rowland, S., Shaw, G., Mandel, R.J., Foster, T.C., Kumar, A., and Sarkisian, M.R. (2016). Type 3 adenylyl cyclase and somatostatin receptor 3 expression persists in aged rat neocortical and hippocampal neuronal cilia. Front Aging Neurosci *8*, 127.

Guemez-Gamboa, A., Coufal, N.G., and Gleeson, J.G. (2014). Primary cilia in the developing and mature brain. Neuron *82*, 511-521.

Guo, J., Otis, J.M., Higginbotham, H., Monckton, C., Cheng, J., Asokan, A., Mykytyn, K., Caspary, T., Stuber, G.D., and Anton, E.S. (2017). Primary cilia signaling shapes the development of interneuronal connectivity. Dev Cell *42*, 286-300 e284.

Guo, J., Otis, J.M., Suciu, S.K., Catalano, C., Xing, L., Constable, S., Wachten, D., Gupton, S., Lee, J., Lee, A.*, et al.* (2019). Primary cilia signaling promotes axonal tract development and is disrupted in Joubert Syndrome-related disorders models. Dev Cell *51*, 759-774 e755.

Hamon, M., Doucet, E., Lefevre, K., Miquel, M.C., Lanfumey, L., Insausti, R., Frechilla, D., Del Rio, J., and Verge, D. (1999). Antibodies and antisense oligonucleotide for probing the distribution and putative functions of central 5-HT6 receptors. Neuropsychopharmacology *21*, 68S-76S.

Handel, M., Schulz, S., Stanarius, A., Schreff, M., Erdtmann-Vourliotis, M., Schmidt, H., Wolf, G., and Hollt, V. (1999). Selective targeting of somatostatin receptor 3 to neuronal cilia. Neuroscience *89*, 909-926.

Hansen, J.N., Kaiser, F., Klausen, C., Stuven, B., Chong, R., Bonigk, W., Mick, D.U., Moglich, A., Jurisch-Yaksi, N., Schmidt, F.I.*, et al.* (2020). Nanobody-directed targeting of optogenetic tools to study signaling in the primary cilium. Elife *9*, e57907.

He, S., Ye, Z., Truong, Q., Shah, S., Du, W., Guo, L., Dobbelaar, P.H., Lai, Z., Liu, J., Jian, T.*, et al.* (2012). The discovery of MK-4256, a potent SSTR3 antagonist as a potential treatment of type 2 diabetes. ACS Med Chem Lett *3*, 484-489.

Heinz, D.A., and Bloodgood, B.L. (2020). Mechanisms that communicate features of neuronal activity to the genome. Curr Opin Neurobiol *63*, 131-136.

Herring, B.E., and Nicoll, R.A. (2016). Long-Term Potentiation: From CaMKII to AMPA receptor trafficking. Annu Rev Physiol *78*, 351-365.

Higginbotham, H., Eom, T.Y., Mariani, L.E., Bachleda, A., Hirt, J., Gukassyan, V., Cusack, C.L., Lai, C., Caspary, T., and Anton, E.S. (2012). Arl13b in primary cilia regulates the migration and placement of interneurons in the developing cerebral cortex. Dev Cell *23*, 925-938.

Higginbotham, H., Guo, J., Yokota, Y., Umberger, N.L., Su, C.Y., Li, J., Verma, N., Hirt, J., Ghukasyan, V., Caspary, T.*, et al.* (2013). Arl13b-regulated cilia activities are essential for polarized radial glial scaffold formation. Nat Neurosci *16*, 1000-1007.

Hilgendorf, K.I., Johnson, C.T., and Jackson, P.K. (2016). The primary cilium as a cellular receiver: organizing ciliary GPCR signaling. Curr Opin Cell Biol *39*, 84-92.

Hoftman, G.D., Datta, D., and Lewis, D.A. (2017). Layer 3 excitatory and inhibitory circuitry in the prefrontal cortex: Developmental trajectories and alterations in schizophrenia. Biol Psychiatry *81*, 862-873.

Humbert, M.C., Weihbrecht, K., Searby, C.C., Li, Y., Pope, R.M., Sheffield, V.C., and Seo, S. (2012). ARL13B, PDE6D, and CEP164 form a functional network for INPP5E ciliary targeting. Proc Natl Acad Sci US A *109*, 19691-19696.

Joseph, A., and Turrigiano, G.G. (2017). All for one but not one for all: Excitatory synaptic scaling and intrinsic excitability are coregulated by CaMKIV, whereas inhibitory synaptic scaling is under independent control. J Neurosci *37*, 6778-6785.

Karunakaran, K.B., Chaparala, S., Lo, C.W., and Ganapathiraju, M.K. (2020). Cilia interactome with predicted protein-protein interactions reveals connections to Alzheimer's disease, aging and other neuropsychiatric processes. Sci Rep *10*, 15629.

Kepecs, A., and Fishell, G. (2014). Interneuron cell types are fit to function. Nature *505*, 318-326.

Koemeter-Cox, A.I., Sherwood, T.W., Green, J.A., Steiner, R.A., Berbari, N.F., Yoder, B.K., Kauffman, A.S., Monsma, P.C., Brown, A., Askwith, C.C.*, et al.* (2014). Primary cilia enhance kisspeptin receptor signaling on gonadotropin-releasing hormone neurons. Proc Natl Acad Sci USA *111*, 10335-10340.

Kumamoto, N., Gu, Y., Wang, J., Janoschka, S., Takemaru, K., Levine, J., and Ge, S. (2012). A role for primary cilia in glutamatergic synaptic integration of adult-born neurons. Nat Neurosci *15*, 399-405, S391.

Larkins, C.E., Aviles, G.D., East, M.P., Kahn, R.A., and Caspary, T. (2011). Arl13b regulates ciliogenesis and the dynamic localization of Shh signaling proteins. Mol Biol Cell *22*, 4694-4703.

Lee, C.H., Song, D.K., Park, C.B., Choi, J., Kang, G.M., Shin, S.H., Kwon, I., Park, S., Kim, S., Kim, J.Y.*, et al.* (2020). Primary cilia mediate early life programming of adiposity through lysosomal regulation in the developing mouse hypothalamus. Nat Commun *11*, 5772.

Lee, J.E., and Gleeson, J.G. (2011). Cilia in the nervous system: linking cilia function and neurodevelopmental disorders. Curr Opin Neurol *24*, 98-105.

Lee, S., Hjerling-Leffler, J., Zagha, E., Fishell, G., and Rudy, B. (2010). The largest group of superficial neocortical GABAergic interneurons expresses ionotropic serotonin receptors. J Neurosci *30*, 16796-16808.

Loktev, A.V., and Jackson, P.K. (2013). Neuropeptide Y family receptors traffic via the Bardet-Biedl syndrome pathway to signal in neuronal primary cilia. Cell Rep *5*, 1316-1329.

Louvi, A., and Grove, E.A. (2011). Cilia in the CNS: the quiet organelle claims center stage. Neuron *69*, 1046-1060.

Lu, H., Toh, M.T., Narasimhan, V., Thamilselvam, S.K., Choksi, S.P., and Roy, S. (2015). A function for the Joubert syndrome protein Arl13b in ciliary membrane extension and ciliary length regulation. Dev Biol *397*, 225-236.

Manning, B.D., and Toker, A. (2017). AKT/PKB Signaling: Navigating the network. Cell *169*, 381-405.

Marley, A., and von Zastrow, M. (2010). DISC1 regulates primary cilia that display specific dopamine receptors. PLoS One *5*, e10902.

Marley, A., and von Zastrow, M. (2012). A simple cell-based assay reveals that diverse neuropsychiatric risk genes converge on primary cilia. PLoS One *7*, e46647.

Mick, D.U., Rodrigues, R.B., Leib, R.D., Adams, C.M., Chien, A.S., Gygi, S.P., and Nachury, M.V. (2015). Proteomics of primary cilia by proximity labeling. Dev Cell *35*, 497-512.

Moffat, J., Grueneberg, D.A., Yang, X., Kim, S.Y., Kloepfer, A.M., Hinkle, G., Piqani, B., Eisenhaure, T.M., Luo, B., Grenier, J.K.*, et al.* (2006). A lentiviral RNAi library for human and mouse genes applied to an arrayed viral high-content screen. Cell *124*, 1283-1298.

Monteiro, P., and Feng, G. (2017). SHANK proteins: roles at the synapse and in autism spectrum disorder. Nat Rev Neurosci *18*, 147-157.

Moore, B.S., Stepanchick, A.N., Tewson, P.H., Hartle, C.M., Zhang, J., Quinn, A.M., Hughes, T.E., and Mirshahi, T. (2016). Cilia have high cAMP levels that are inhibited by Sonic Hedgehog-regulated calcium dynamics. Proc Natl Acad Sci USA *113*, 13069-13074.

Mukherjee, S., Jansen, V., Jikeli, J.F., Hamzeh, H., Alvarez, L., Dombrowski, M., Balbach, M., Strunker, T., Seifert, R., Kaupp, U.B.*, et al.* (2016). A novel biosensor to study cAMP dynamics in cilia and flagella. Elife *5*, e14052.

Mukhopadhyay, S., Wen, X., Ratti, N., Loktev, A., Rangell, L., Scales, S.J., and Jackson, P.K. (2013). The ciliary G-protein-coupled receptor Gpr161 negatively regulates the Sonic hedgehog pathway via cAMP signaling. Cell *152*, 210-223.

Mykytyn, K., and Askwith, C. (2017). G-protein-coupled receptor signaling in cilia. Cold Spring Harb Perspect Biol *9*, a028183.

Nachury, M.V. (2018). The molecular machines that traffic signaling receptors into and out of cilia. Curr Opin Cell Biol *51*, 124-131.

Najafi, M., and Calvert, P.D. (2012). Transport and localization of signaling proteins in ciliated cells. Vision Res *75*, 11-18.

Nelson, S.B., and Valakh, V. (2015). Excitatory/Inhibitory balance and circuit homeostasis in autism spectrum disorders. Neuron *87*, 684-698.

Novarino, G., Akizu, N., and Gleeson, J.G. (2011). Modeling human disease in humans: the ciliopathies. Cell *147*, 70-79.

O'Donovan, M.C., Craddock, N., Norton, N., Williams, H., Peirce, T., Moskvina, V., Nikolov, I., Hamshere, M., Carroll, L., Georgieva, L.*, et al.* (2008). Identification of loci associated with schizophrenia by genome-wide association and follow-up. Nat Genet *40*, 1053-1055.

Pazour, G.J., Dickert, B.L., Vucica, Y., Seeley, E.S., Rosenbaum, J.L., Witman, G.B., and Cole, D.G. (2000). *Chlamydomonas* IFT88 and its mouse homologue, polycystic kidney disease gene *tg737*, are required for assembly of cilia and flagella. J Cell Biol *151*, 709-718.

Plotnikova, O.V., Seo, S., Cottle, D.L., Conduit, S., Hakim, S., Dyson, J.M., Mitchell, C.A., and Smyth, I.M. (2015). INPP5E interacts with AURKA, linking phosphoinositide signaling to primary cilium stability. J Cell Sci *128*, 364-372.

Pratt, K.G., Taft, C.E., Burbea, M., and Turrigiano, G.G. (2008). Dynamics underlying synaptic gain between pairs of cortical pyramidal neurons. Dev Neurobiol *68*, 143-151.

Pratt, K.G., Watt, A.J., Griffith, L.C., Nelson, S.B., and Turrigiano, G.G. (2003). Activity-dependent remodeling of presynaptic inputs by postsynaptic expression of activated CaMKII. Neuron *39*, 269-281.

Reiter, J.F., and Leroux, M.R. (2017). Genes and molecular pathways underpinning ciliopathies. Nat Rev Mol Cell Biol *18*, 533-547.

Rhee, S., Kirschen, G.W., Gu, Y., and Ge, S. (2016). Depletion of primary cilia from mature dentate granule cells impairs hippocampus-dependent contextual memory. Sci Rep *6*, 34370.

RK, C.Y., Merico, D., Bookman, M., J, L.H., Thiruvahindrapuram, B., Patel, R.V., Whitney, J., Deflaux, N., Bingham, J., Wang, Z.*, et al.* (2017). Whole genome sequencing resource identifies 18 new candidate genes for autism spectrum disorder. Nat Neurosci *20*, 602-611.

Rohrer, S.P., Birzin, E.T., Mosley, R.T., Berk, S.C., Hutchins, S.M., Shen, D.M., Xiong, Y., Hayes, E.C., Parmar, R.M., Foor, F.*, et al.* (1998). Rapid identification of subtype-selective agonists of the somatostatin receptor through combinatorial chemistry. Science *282*, 737-740.

Rohrer, S.P., and Schaeffer, J.M. (2000). Identification and characterization of subtype selective somatostatin receptor agonists. J Physiol Paris *94*, 211-215.

Schou, K.B., Pedersen, L.B., and Christensen, S.T. (2015). Ins and outs of GPCR signaling in primary cilia. EMBO Rep *16*, 1099-1113.

Schulz, S., Handel, M., Schreff, M., Schmidt, H., and Hollt, V. (2000). Localization of five somatostatin receptors in the rat central nervous system using subtype-specific antibodies. J Physiol Paris *94*, 259-264.

Sipos, E., Komoly, S., and Acs, P. (2018). Quantitative comparison of primary cilia marker expression and length in the mouse brain. J Mol Neurosci *64*, 397-409.

Sohal, V.S., and Rubenstein, J.L.R. (2019). Excitation-inhibition balance as a framework for investigating mechanisms in neuropsychiatric disorders. Mol Psychiatry *24*, 1248-1257.

Spassky, N., Han, Y.G., Aguilar, A., Strehl, L., Besse, L., Laclef, C., Ros, M.R., Garcia-Verdugo, J.M., and Alvarez-Buylla, A. (2008). Primary cilia are required for cerebellar development and Shh-dependent expansion of progenitor pool. Dev Biol *317*, 246-259.

Stanic, D., Malmgren, H., He, H., Scott, L., Aperia, A., and Hokfelt, T. (2009). Developmental changes in frequency of the ciliary somatostatin receptor 3 protein. Brain Res *1249*, 101-112.

Sterpka, A., and Chen, X. (2018). Neuronal and astrocytic primary cilia in the mature brain. Pharmacol Res *137*, 114-121.

Su, S., Phua, S.C., Derose, R., Chiba, S., Narita, K., Kalugin, P.N., Katada, T., Kontani, K., Takeda, S., and Inoue, T. (2013). Genetically encoded calcium indicator illuminates calcium dynamics in primary cilia. Nat Methods *10*, 1105-1107.

Tatavarty, V., Torrado Pacheco, A., Groves Kuhnle, C., Lin, H., Koundinya, P., Miska, N.J., Hengen, K.B., Wagner, F.F., Van Hooser, S.D., and Turrigiano, G.G. (2020). Autism-associated Shank3 is essential for homeostatic compensation in rodent V1. Neuron *106*, 769-777 e764.

Torri, F., Akelai, A., Lupoli, S., Sironi, M., Amann-Zalcenstein, D., Fumagalli, M., Dal Fiume, C., Ben-Asher, E., Kanyas, K., Cagliani, R.*, et al.* (2010). Fine mapping of AHI1 as a schizophrenia susceptibility gene: from association to evolutionary evidence. FASEB J *24*, 3066-3082.

Tremblay, R., Lee, S., and Rudy, B. (2016). GABAergic interneurons in the neocortex: From cellular properties to circuits. Neuron *91*, 260-292.

Trojanowski, N.F., Bottorrf, J., and Turrigiano, G.G. (2020). Activity labeling in vivo using CAMPARI2 reveals electrophysiological differences between neurons with high and low firing rate set points. Neuron. *In press.*

Turrigiano, G.G. (2017). The dialectic of Hebb and homeostasis. Philos Trans R Soc Lond B Biol Sci *372*.

Turrigiano, G.G., Leslie, K.R., Desai, N.S., Rutherford, L.C., and Nelson, S.B. (1998). Activity-dependent scaling of quantal amplitude in neocortical neurons. Nature *391*, 892-896.

Turrigiano, G.G., and Nelson, S.B. (2000). Hebb and homeostasis in neuronal plasticity. Curr Opin Neurobiol *10*, 358-364.

Tuson, M., He, M., and Anderson, K.V. (2011). Protein kinase A acts at the basal body of the primary cilium to prevent Gli2 activation and ventralization of the mouse neural tube. Development *138*, 4921-4930.

Urban-Ciecko, J., and Barth, A.L. (2016). Somatostatin-expressing neurons in cortical networks. Nat Rev Neurosci *17*, 401-409.

Valente, E.M., Rosti, R.O., Gibbs, E., and Gleeson, J.G. (2014). Primary cilia in neurodevelopmental disorders. Nat Rev Neurol *10*, 27-36.

Verpelli, C., Dvoretskova, E., Vicidomini, C., Rossi, F., Chiappalone, M., Schoen, M., Di Stefano, B., Mantegazza, R., Broccoli, V., Bockers, T.M.*, et al.* (2011). Importance of Shank3 protein in regulating metabotropic glutamate receptor 5 (mGluR5) expression and signaling at synapses. J Biol Chem *286*, 34839-34850.

Wang, Z., Phan, T., and Storm, D.R. (2011). The type 3 adenylyl cyclase is required for novel object learning and extinction of contextual memory: role of cAMP signaling in primary cilia. J Neurosci *31*, 5557-5561.

West, A.E., and Greenberg, M.E. (2011). Neuronal activity-regulated gene transcription in synapse development and cognitive function. Cold Spring Harb Perspect Biol *3*, a005744.

Willaredt, M.A., Hasenpusch-Theil, K., Gardner, H.A., Kitanovic, I., Hirschfeld-Warneken, V.C., Gojak, C.P., Gorgas, K., Bradford, C.L., Spatz, J., Wolfl, S.*, et al.* (2008). A crucial role for primary cilia in cortical morphogenesis. J Neurosci *28*, 12887-12900.

Wray, N.R., Pergadia, M.L., Blackwood, D.H., Penninx, B.W., Gordon, S.D., Nyholt, D.R., Ripke, S., MacIntyre, D.J., McGhee, K.A., Maclean, A.W.*, et al.* (2012). Genome-wide association study of major depressive disorder: new results, meta-analysis, and lessons learned. Mol Psychiatry *17*, 36-48.

Xu, X., Roby, K.D., and Callaway, E.M. (2010). Immunochemical characterization of inhibitory mouse cortical neurons: three chemically distinct classes of inhibitory cells. J Comp Neurol *518*, 389-404.

Yao, G., Luo, C., Harvey, M., Wu, M., Schreiber, T.H., Du, Y., Basora, N., Su, X., Contreras, D., and Zhou, J. (2016). Disruption of polycystin-L causes hippocampal and thalamocortical hyperexcitability. Hum Mol Genet *25*, 448-458.

Yap, E.L., and Greenberg, M.E. (2018). Activity-regulated transcription: Bridging the gap between neural activity and behavior. Neuron *100*, 330-348.

Youn, Y.H., and Han, Y.G. (2018). Primary cilia in brain development and diseases. Am J Pathol *188*, 11-22.

Yu, H., Su, Y., Shin, J., Zhong, C., Guo, J.U., Weng, Y.L., Gao, F., Geschwind, D.H., Coppola, G., Ming, G.L.*, et al.* (2015). Tet3 regulates synaptic transmission and homeostatic plasticity via DNA oxidation and repair. Nat Neurosci *18*, 836-843.

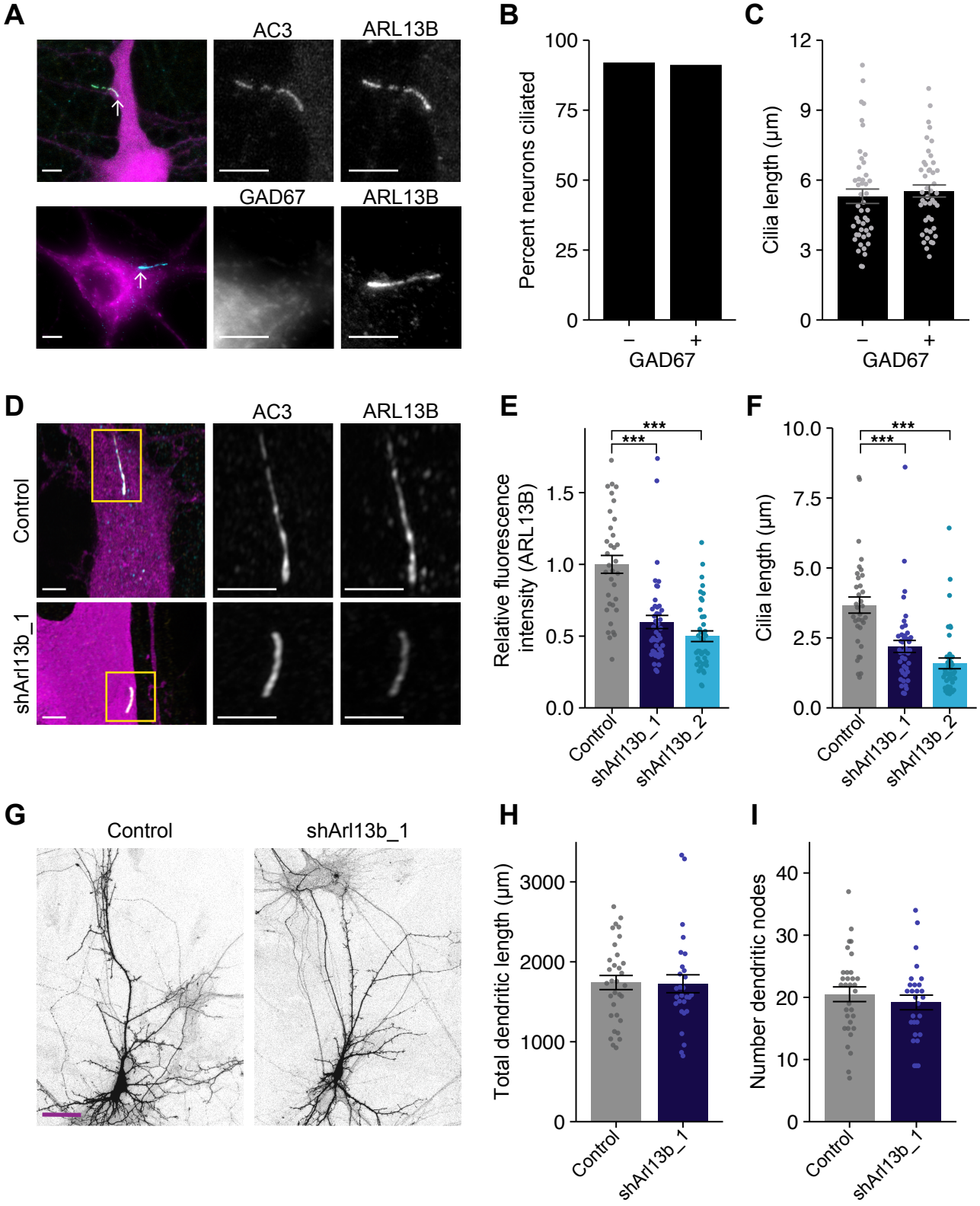

Tereshko et al.,
Figure 1

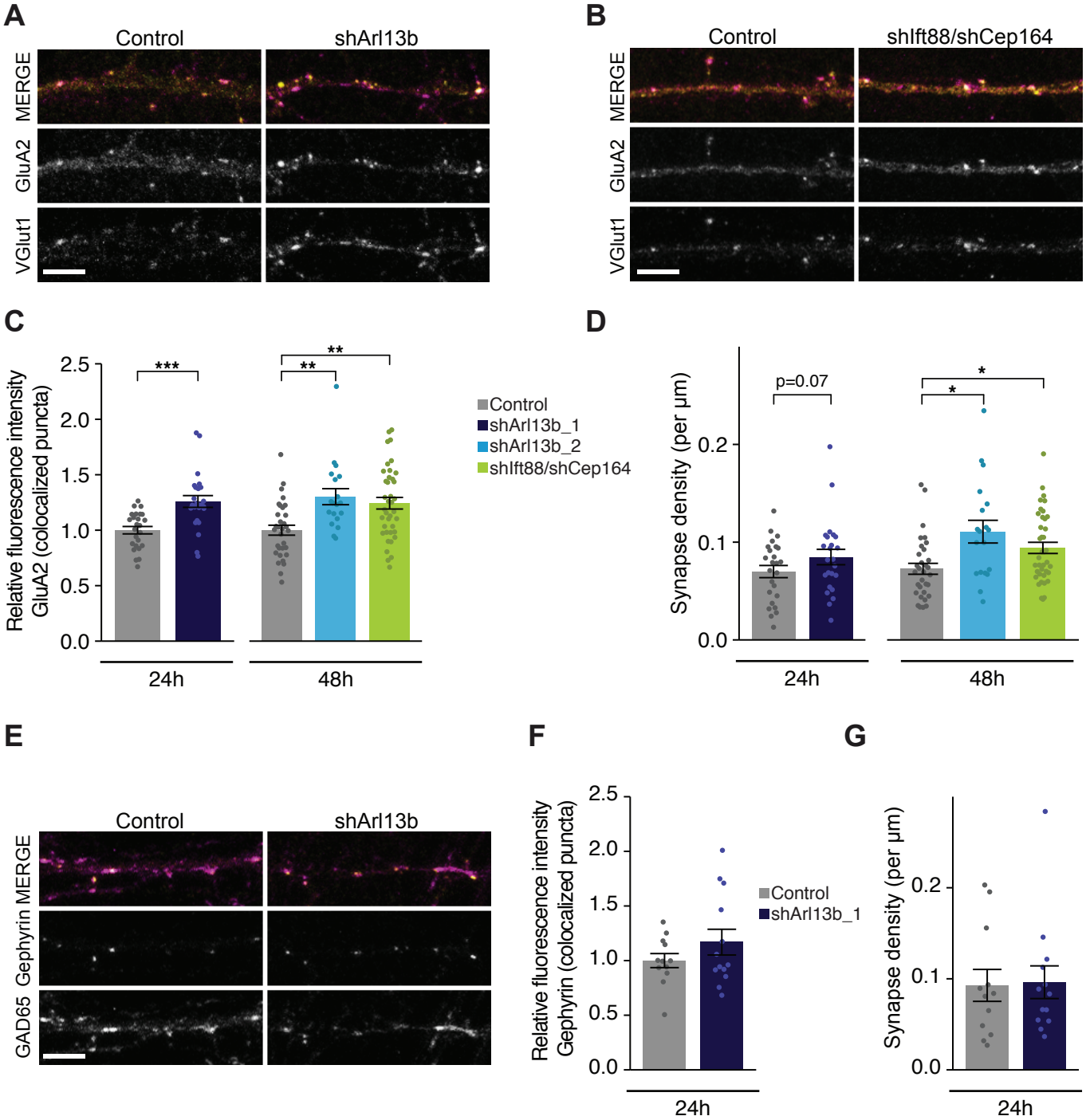

Tereshko et al.,
Figure 2

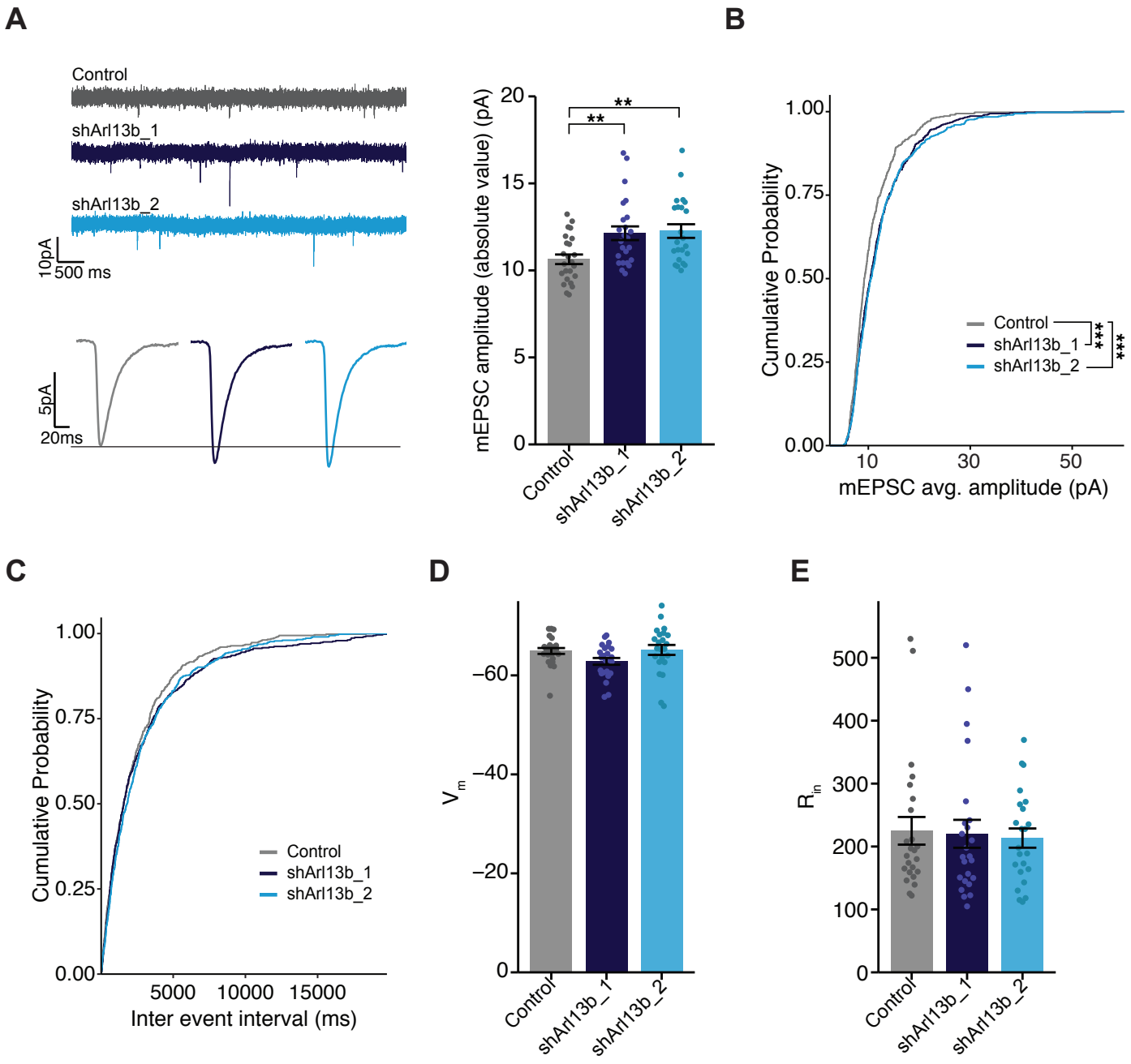

Tereshko et al.,
Figure 3

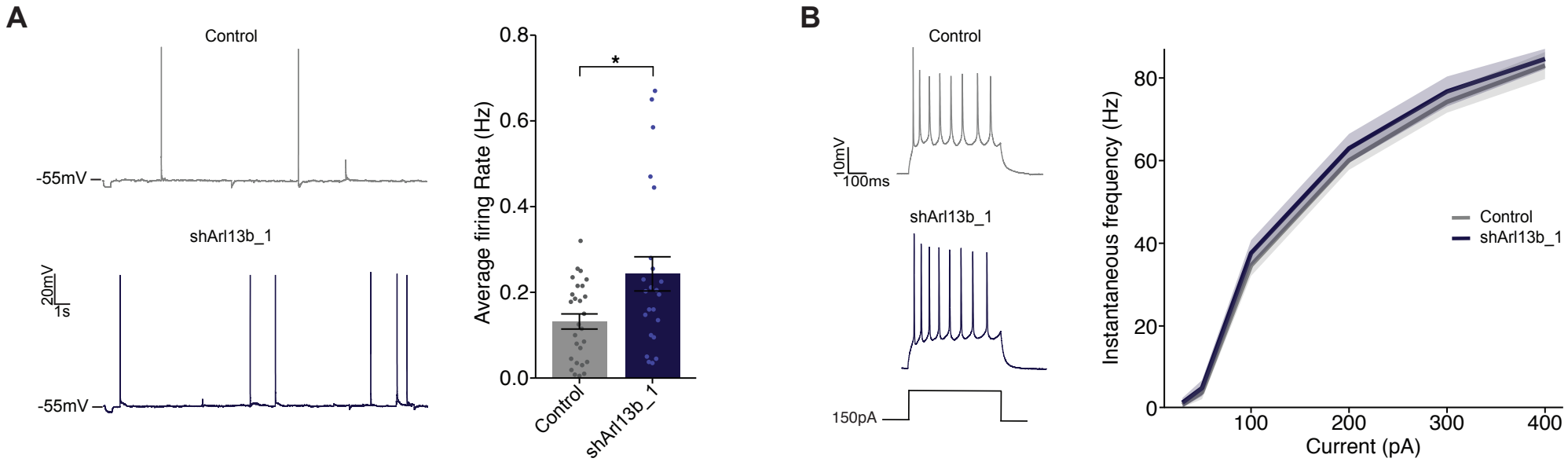

Tereshko et al.,
Figure 4

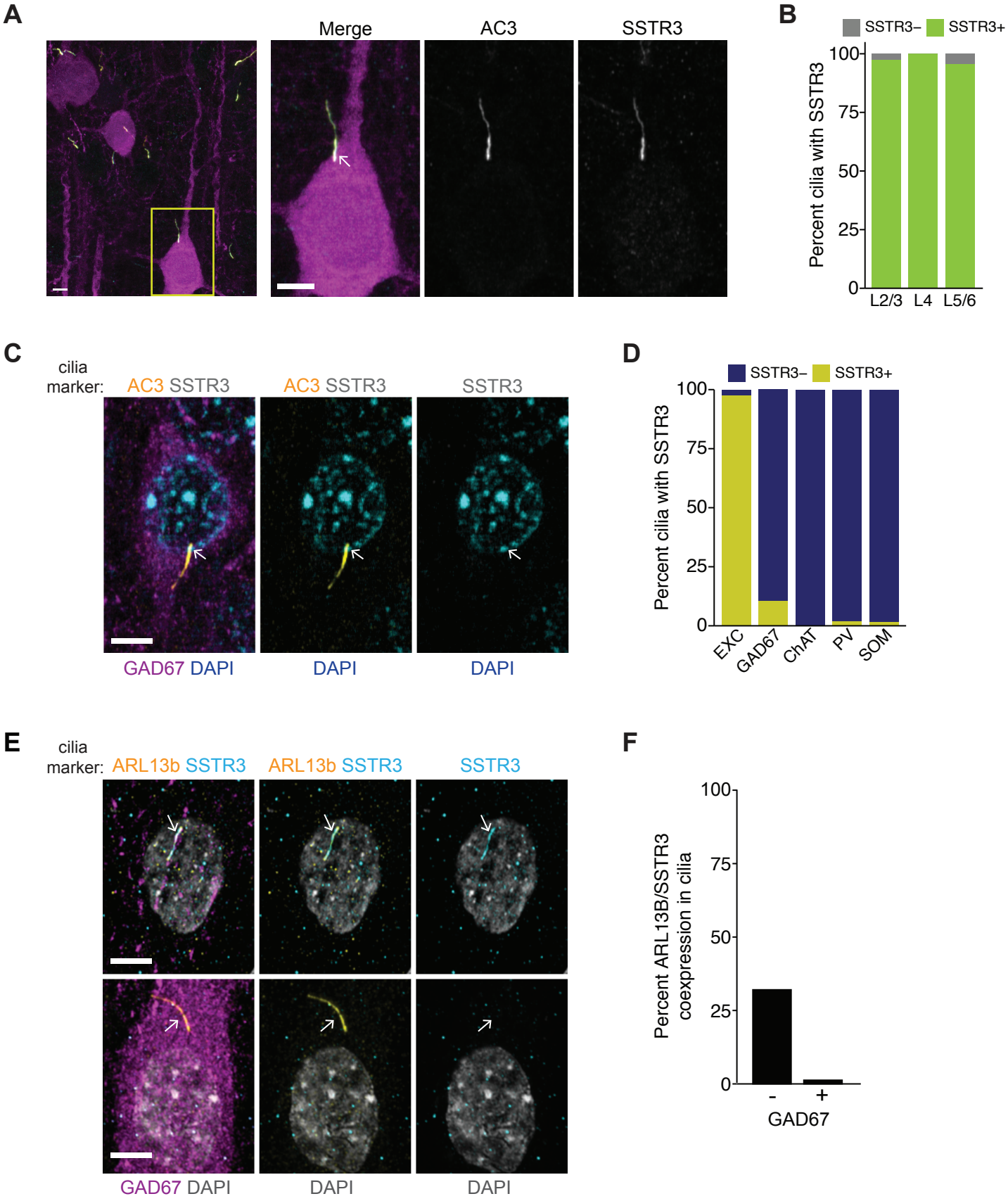

Tereshko et al., Figure 5

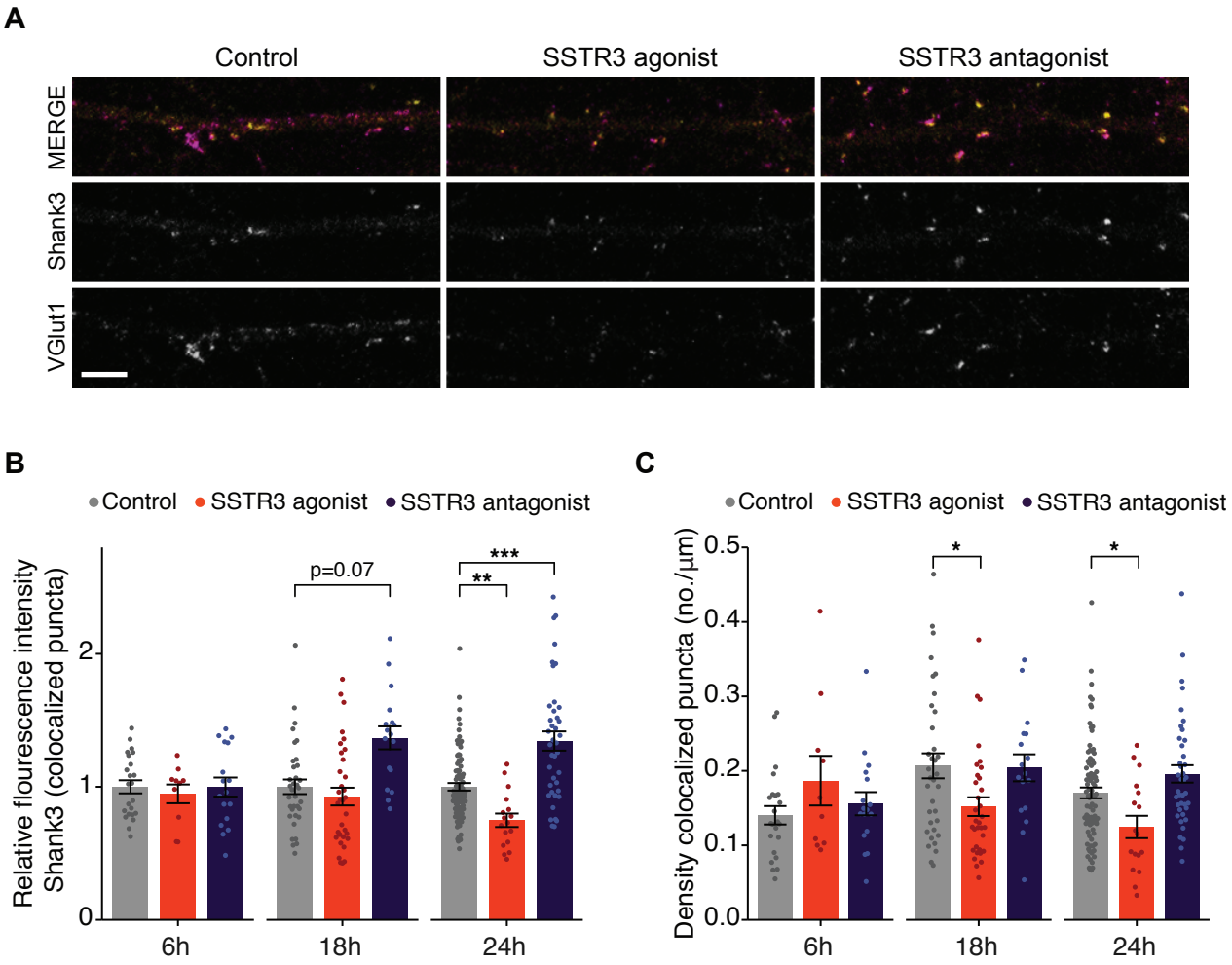

Tereshko et al.,
Figure 6